Supplement of

Soil–atmosphere water vapor exchange in semi-arid Northwest China: New insights from fiber-optic relative humidity sensing

Junyi Guo[1], Mengya Sun[2], Chengcheng Zhang[1], Jie Liu[3], Qingnan Lou[1], Qiyu Xu[1], and Bin Shi[1]

[1]School of Earth Sciences and Engineering, Nanjing University, Nanjing, 210023, China
[2]School of Earth Sciences and Engineering, Hohai University, Nanjing, 210023, China
[3]Huairou Laboratory, Beijing, China

Correspondence to: Bin Shi (shibin@nju.edu.cn)

Contents of this file

Text S1. Simultaneous measurement of temperature and relative humidity using an FBG-based relative humidity sensor

FBG technology is a common quasi-distributed fiber-optic sensing technique for monitoring temperature and strain, as shown in Figure S2:

$$\frac{\Delta\lambda}{\lambda_{\mathrm{B}}} = (1-\mathrm{Pe})\varepsilon_z + (\alpha_{\mathrm{F}} + \zeta_{\mathrm{F}})\Delta T \tag{1}$$

where $\Delta\lambda$ is the Bragg wavelength change, P_e is the photo-elastic constant of the fiber, ε_Z is the strain induced on the fiber, α_F is the thermal expansion coefficient of the fiber, ζ_F is the fiber thermo-optic coefficient, and ΔT is the temperature change.

FBG is not inherently sensitive to relative humidity. However, relative humidity sensing can be achieved by coating the optical fiber with polyimide (PI), a moisture-sensitive material. When ambient humidity changes, polyimide interacts with water molecules in the air, resulting in its expansion or contraction. This dimensional change induces axial strain in the FBG, causing a shift in its Bragg wavelength corresponding to the change in humidity, as shown in Figure S3. Temperature compensation is used to eliminate the interference of temperature fluctuation on FBG wavelength. The most common solution is to introduce an uncoated FBG(B-FBG) for temperature sensing only, and placed in the same environment as PI-FBG, then the measured relative humidity and temperature is:

$$RH = \frac{\Delta\lambda_1 - \Delta\lambda_2 K_{T1} / K_{T2}}{K_{RH}} + RH_0 \tag{2}$$

$$T = \frac{\Delta\lambda_2}{K_{T2}} + T_0 \tag{3}$$

where K_{T1} and K_{T2} are respectively the temperature sensitivity coefficients of the PI-FBG and B-FBG, K_{RH} is the humidity sensitivity coefficient of the PI-FBG, $\Delta\lambda_1$ and $\Delta\lambda_2$ are respectively the Bragg wavelength shifts of the PI-FBG and B-FBG, and RH_0 and T_0 are respectively the relative humidity and temperature corresponding to the initial Bragg wavelength of the PI-FBG and B-FBG.

Text S2. Vertical water vapor flux calculation

Relative humidity is defined as the ratio of the water vapor density (ρ_v) of a solution to the water vapor density of free water ($\rho_{v,sat}$) at the same temperature in equilibrium. It is also expressed as the ratio of the water vapor pressure (u_v) in the air to the saturation vapor pressure ($u_{v,sat}$) at the same temperature, typically presented as a percentage:

$$RH = \frac{\rho_{\mathrm{v}}}{\rho_{\mathrm{v,sat}}} = \frac{u_{\mathrm{v}}}{u_{\mathrm{v,sat}}} \tag{4}$$

Tetens (1930) proposed an empirical equation relating saturation vapor pressure ($u_{v,sat}$) to temperature (T) of water:

$$u_{\mathrm{v,sat}} = 0.611\exp(17.27\frac{T-273.12}{T-36}) \tag{5}$$

According to the ideal gas law, the water vapor density (ρ_{v}) can be calculated, as follows:

$$\rho_{\mathrm{v}} = \frac{u_{\mathrm{v}}\omega_{\mathrm{v}}}{RT} = \frac{u_{\mathrm{v,sat}}\omega_{\mathrm{v}}}{RT}RH = \frac{0.611\exp(17.27\frac{T-273.12}{T-36})\bullet\omega_{\mathrm{v}}}{RT}RH \tag{6}$$

The fundamental driving mechanism for vapor flow in unsaturated soil is the gradient in the chemical potential of water vapor, typically expressed as water vapor density (ρ_v).

$$q_{\mathrm{v}} = -D_{\mathrm{v}}\nabla\rho_{\mathrm{v}} \tag{7}$$

where D_{v} is the diffusion coefficient of water vapor transport in unsaturated soil (m^2/s).

The vertical water vapor flux between adjacent depths x1 and x2 in unsaturated soil by molecular diffusion is represented in the following equation:

$$q_{\mathrm{v}} = \Theta_{\mathrm{a}}\tau\frac{\mathrm{D}_1\rho_{\mathrm{v1}} - \mathrm{D}_2\rho_{\mathrm{v2}}}{\mathrm{x}_1 - \mathrm{x}_2} \tag{8}$$

where D_1 and D_2 are the diffusion coefficients of water vapor in air at local temperatures of x_1 and x_2, ρ_{v1} and ρ_{v2} are the water vapor densities at depths x_1 and x_2, respectively, τ is the dimensionless tortuosity factor that accounts for the increased diffusion path length (here taken as 0.66), and Θ_a is the air filled porosity accounting for the reduced cross-sectional area for vapor flow caused by liquid and solid components in the soil.

Table S1. Basic Physical Properties of Loess in Yan'an.

Grain Size Distribution			Atterberg Limits		
Sand (%)	Silt (%)	Clay (%)	Liquid Limit (%)	Plastic Limit (%)	Plasticity Index (%)
3.06	90.83	6.11	27.3	18.1	9.2

Table S2. Technical specifications of the PI-FBG Sensor.

Parameter	PI-FBG humidity sensor
Temperature measurement range	-40–80 ℃
Temperature measurement accuracy	±0.1 ℃
Temperature resolution	0.01 ℃
Humidity measurement range	11.3–97.3%RH
Humidity measurement accuracy	±1%RH
Humidity resolution	0.05%RH
Probe size	65 mm (long) * 12 mm (diameter)
Probe structure	Closed, stainless steel
Probe protection type	Waterproof and dustproof

Table S3. Characteristics parameters of PI-FBG.

Characteristics parameters	Values
Reflectivity	≥50%
FWHM (Typical value)	300 pm
Min Max variation within array	3 dB
Centre wavelength	1510 nm to 1590 nm
Absolute wavelength accuracy	≤0.5 nm
Relative wavelength accuracy	≤0.5 nm
Grating length	~4 mm
Grating type	Uniform apodized
Side lobe suppression ratio	≥10 dB
Grating separation (center to center)	≥5 mm
Fiber coating	Polymide
Core diameter	10.4 μm
Cladding diameter	125 μm
Coating diameter	155±5 μm
Numerical aperture	0.11-0.44
Fiber attenuation	≤0.6 dB/km
Temperature operating range	-55 to 300 ℃
Typical tensile strength FSG	> 4GPa(~5% strain)

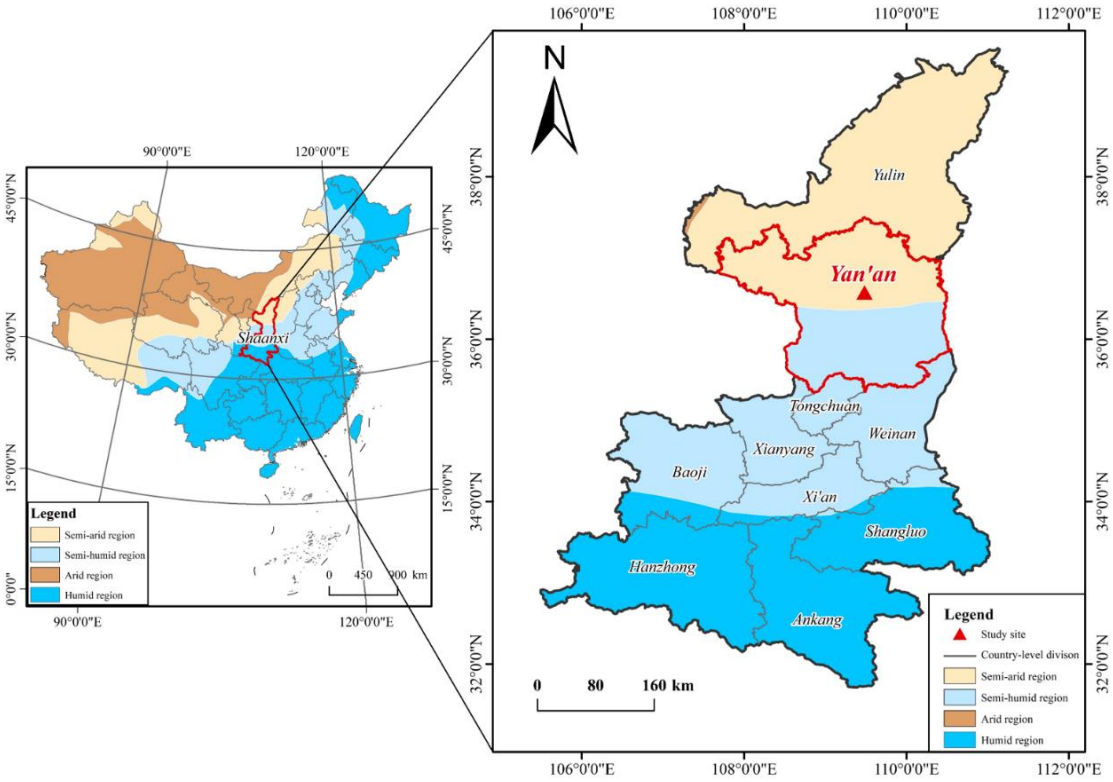

Figure S1. Study area in the semi-arid region of Yan'an, Shaanxi Province, China. Left: Distribution of arid and semi-arid regions across China, primarily concentrated in the northwest, north, and parts of the southwest, covering approximately one-third of the country's land area. Right: Location of the study site within Shaanxi Province. Arid and semi-arid regions in the province are mainly distributed across the northern Loess Plateau and parts of the central Guanzhong Plain. The specific monitoring site is situated in the semi-arid zone of the northern Loess Plateau. The base map was obtained from the Standard Map Service of the Ministry of Natural Resources (map number GS(2024)0650), with no modifications made to administrative boundaries.

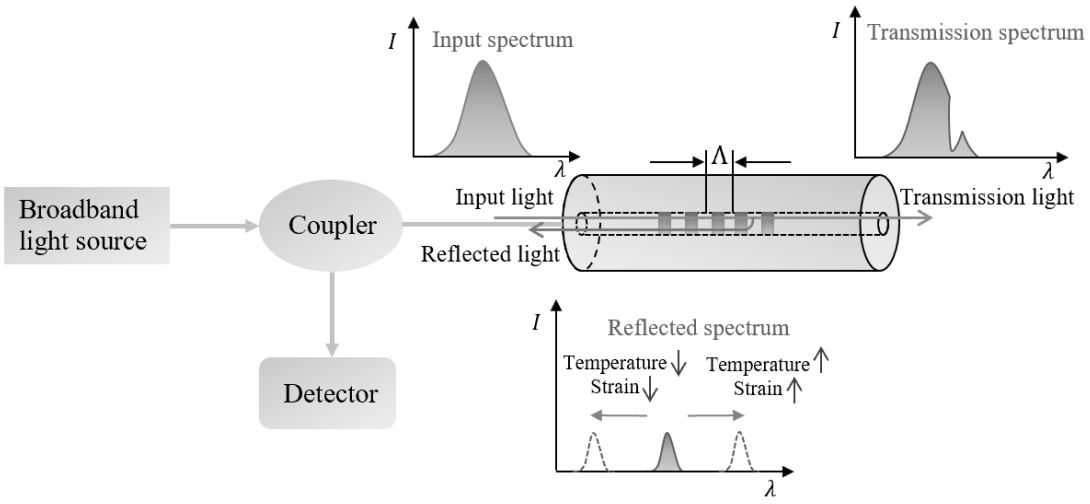

Figure S2. Schematic diagram of FBG sensing principle. The FBG is a periodic modulation of the refractive index inside the core of an optical fiber. When a broad band pulse is spread down the FBG which serves as a wavelength selective filter, the most is transmitted and a light signal with a specific wavelength is reflected called the Bragg wavelength (λ_B). λ_B is dependent on the effective refractive index of the fiber core (n_{eff}) and the spatial period of the grating (Λ). The variation of temperature and strain experienced by the FBG has an impact on n_{eff} and Λ , leading to a shift in Bragg wavelength.

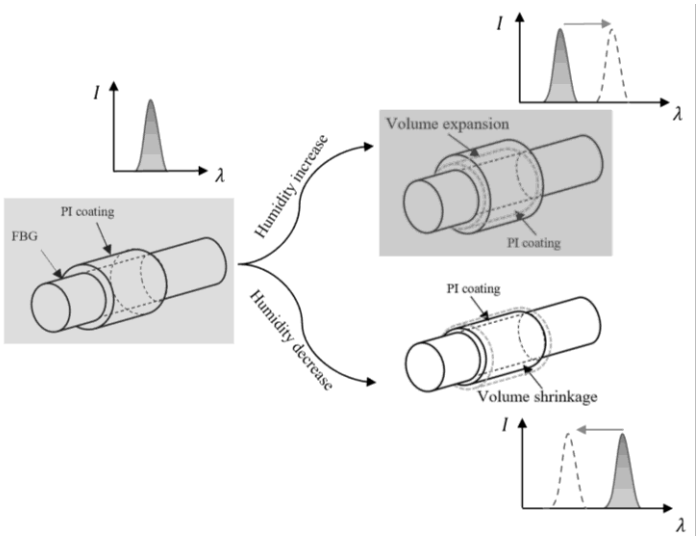

Figure S3. PI-FBG humidity sensing principle. PI contains hydrophilic groups that can interact with water molecules to form hydrogen bonds to achieve water absorption. With the increase of humidity, the number of adsorbed water molecules inside the PI will increase, inducing the increase of the PI volume, so the PI film appears linear expansion phenomenon. The volume change of PI induces a mechanical effect on the FBG, which has a significant influence on the shift of Bragg wavelength (Fig. 1).

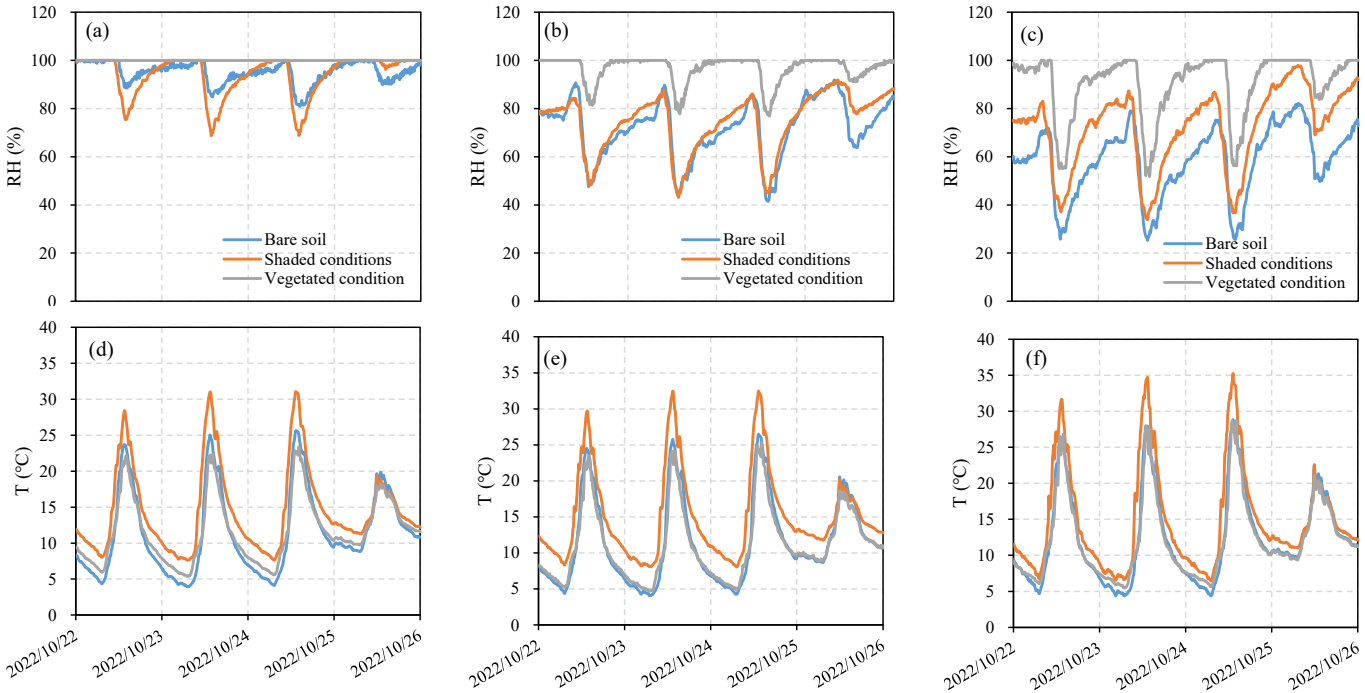

Figure S4. Comparison of relative humidity and temperature measured by sensors installed at different vertical positions: Panels (a)–(c) show relative humidity at 7 mm below the soil surface, at the soil–atmosphere interface, and 1 cm above the interface, respectively; panels (d)–(f) present the corresponding temperature measurements. A comprehensive analysis indicates that vegetated areas consistently exhibit the highest relative humidity, likely due to the combined effects of reduced direct solar radiation and sustained transpiration, which help maintain elevated moisture levels. In contrast, the highest temperatures were recorded in shaded zones without direct solar exposure, suggesting that the absence of radiative cooling plays a critical role in temperature retention. These humidity–temperature distribution patterns provide insights into microclimatic variations across different surface exposures. Although not discussed in detail in the main text, these observations highlight the variability in microclimatic conditions and surface responses to environmental drivers, offering valuable reference data for future research on soil–atmosphere heat and moisture exchange processes.

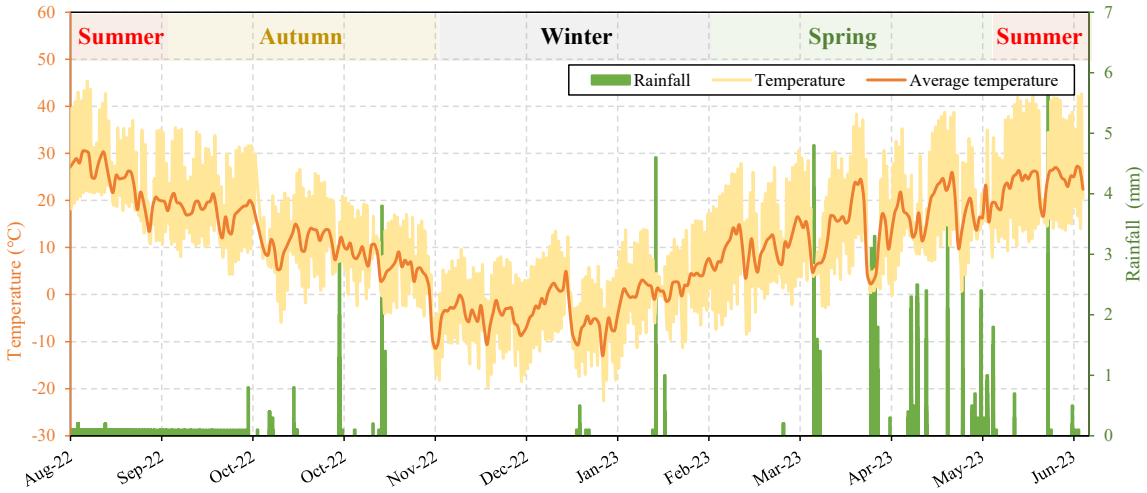

Figure S5. Temperature and rainfall at the study site from August 2022 to June 2023, recorded at 1-hour intervals by the weather station.